1. Further Model Description

The ice sheet-shelf model uses a finite-difference Arakawa-C grid, where horizontal velocities (*u,v*) are calculated on separate grids staggered by half a grid box relative to ice thickness (*h)* (Fig. S1)[38].

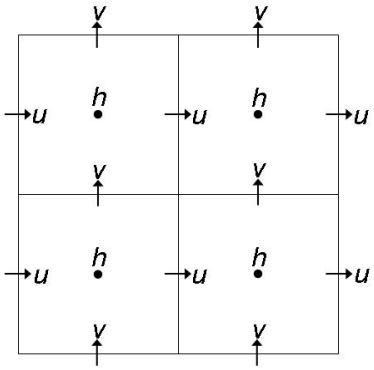

Figure S1. Finite-difference staggered grids in the ice sheet-shelf model. *h* denotes the centers of h-grid boxes, where ice thickness, ice temperatures, and bedrock elevations are calculated. *u* and *v* denote the staggered grid points where horizontal velocity components are calculated.

The equations and method of solution for horizontal velocities are described in detail in Pollard and DeConto[12], including the heuristic, iterative combination of the two sets of scaled equations for terrestrial sheet (Shallow-Ice Approximation, SIA) and marine shelf flows. Although the combined equations can be combined everywhere in the domain, it is faster computationally to only calculate shelf flow in restricted regions – where the basal sliding coefficient is large (slippery beds or floating), or even simpler, only where floating. We have used the latter approach for most simulations here, i.e., allowing shelf flow only where floating. In Supplementary Information (SI) section 8 we show that the long-term results are essentially unchanged by allowing combined flow in grounded areas.

Schoof[5] has shown that to capture grounding-line migration accurately, it is necessary to either resolve the grounding -zone boundary layer at very fine resolution (~0.1 km), or to apply an analytic constraint on the flux across the grounding line. Otherwise, coarse-grid models fail to capture basic aspects of grounding line movement in idealized tests[39,40]. Here, we calculate the flux q_g across model grounding lines as in Schoof[5] (his Eq. 29):

$$q_g = \left(\frac{\overline{A}(\rho_i g)^{n+1}(1-\rho_i/\rho_w)^n}{4^n C'} \right)^{\frac{1}{m'+1}} \left(\frac{\tau_{xx}}{\tau_f} \right)^{\frac{n}{m'+1}} \left(h_g^{\frac{m'+n+3}{m'+1}} \right) \quad \text{(S1)}$$

This yields the vertically

averaged velocity $u_g = q_g/h_g$ where h_g is the ice thickness at the grounding line. The middle term in Eq. (S1) accounts for back stress at the grounding line due to buttressing by downstream islands, pinning points or side-shear, where τ_{xx} is the longitudinal stress across the grounding line from the solution of the shelf-flow equation in the previous iteration, and τ_f is the same quantity in the absence of any buttressing, given by $0.5\ \rho_i\ g\ h_g\ (1-\rho_i/\rho_w)$. Other symbols are as in Schoof[5] and Pollard and DeConto[12]: A is the depth-averaged ice rheological coefficient and n is the Glen-Law exponent, C' is Schoof's[5] basal sliding coefficient and m' the basal sliding exponent, corresponding to $B^{-1/m}$ and $1/m$ here and in Pollard and DeConto[12], due to the reversed form of the basal sliding law (Eq. (S2) below). ρ_i and ρ_w are densities of ice and water respectively, and g is the gravitational acceleration. h_g is interpolated in space by first estimating the sub-grid position of the grounding line between the two surrounding floating and grounded h-grid points. This is done by linearly interpolating height-above-flotation between those two points to where it is zero (cf. Pattyn et al.[41]), linearly interpolating bedrock elevation to that location, and then simply computing the flotation thickness of ice for that bedrock elevation and current sea level.

The velocity u_g is calculated at the grounding-line points on the u-grid, i.e., those with floating ice in one adjacent (left or right) h-grid box and grounded ice in the other (and similarly for v_g on the v-grid). These velocities are imposed as an internal boundary condition for the shelf-flow equations, in effect overriding the large-scale velocity solution at the grounding line. Note that this procedure only considers one-dimensional dynamics perpendicular to the grounding line (as in the 1-D flowline analysis in Schoof[5]). This works naturally with the staggered C-grid (Fig. S1), where the grounding "line" is a continuous series of perpendicular segments of u-direction or v-direction interfaces between h-grid boxes, and u_g (v_g) velocities flow across interfaces running through u-grid (v-grid) points. We neglect spatial gradients parallel to the grounding line, which are not included in the derivation of Eq. (S1); however, they are considered to cause only small second-order effects in typical 2-D flows (C. Schoof, pers. comm.).

We have tested this method of solution in many idealized 1-D flowline tests, similar to those in Schoof[5]. Our goal was to achieve the same grounding-migration results using a coarse grid (~10 to 40 km) with those using very fine-grids (~0.1 km). For grids coarser than ~ 1 km, we find that it is necessary to impose Eq. (S1) as a grounding-line boundary condition. For grids coarser than a few km, we find that an additional rule is necessary, because the outer-solution structure of the grounding zone is not fully captured by the grid:

> If the flux q_g from Eq. (S1) is greater than the large-scale shelf-equation's flux q_m at the grounding line, then u_g (= q_g/h_g) is imposed exactly at the u-grid grounding-line point; conversely if $q_g < q_m$, then u_g is imposed one u-grid box downstream of the grounding-line point. The former is usually associated with grounding-line retreat, and the latter usually with grounding-line advance.

With this rule and 10 to 40 km grids, grounding line retreats and advances are captured correctly in large suites of idealized 1-D flowline tests, many as part of the MISMIP

model intercomparison[39,40]. They include forward and reverse-sloping bedrocks and transient sea-level changes, and our results agree well with those using very fine (~0.1 km) grids and with analytical solutions[5].

Ice thickness advection is treated by an ADI (alternating-direction-implicit) scheme that includes linearized time-implicit tendencies for all SIA terms, and uses time-explicit shelf-flow velocities. Ice temperatures are advected using upstream parabolic interpolation[42], allowing for vertical heat diffusion, geothermal heat flux, basal freezing or melting, and frictional heating by vertical (SIA-flow) shearing, horizontal (shelf-flow) shearing and basal sliding. Geothermal heat flux is set to .070 W m^{-2} for West Antarctica, and .0546 W m^{-2} elsewhere[43]. Basal sliding velocities u_b are related to basal stress τ_b as in Pollard and DeConto[12]:

$$\vec{u}_b = B\left|\tau_b\right|^{m-1}\vec{\tau}_b \qquad \text{(S2)}$$

with $m = 2$. Where basal temperatures are at the pressure melting point, the basal sliding coefficient B is set to either 10^{-10} m a^{-1} Pa^{-2} (typical of hard bedrock) or 10^{-6} m a^{-1} Pa^{-2} (typical of deformable sediment). Sediment is assumed to exist where today's rebounded ice-free BEDMAP[1] topography lies below sea level, as a simple attempt at prescribing the large-scale sediment distribution. Additionally, for all runs shown here, B is set to an intermediate value of 10^{-8} m a^{-1} Pa^{-2} in a rectangle roughly corresponding to the Pine Island/Thwaites drainage basin, to achieve more realistic modern grounding lines in that region of the Amundsen Sea. Further adjustments to West Antarctic's B values in sensitivity tests are discussed in SI section 7. As basal temperatures fall below the pressure melt point from 0 to -0.5°C, B is ramped towards essentially zero (10^{-20}, linearly with respect to log(B)), i.e., no sliding if grounded ice is frozen to the bed. However, no such temperature adjustment to B is made at grounding lines, under the assumption that basal ice in the grounding-line boundary layer is always very close to melting.

2. Simulation of Modern Antarctica

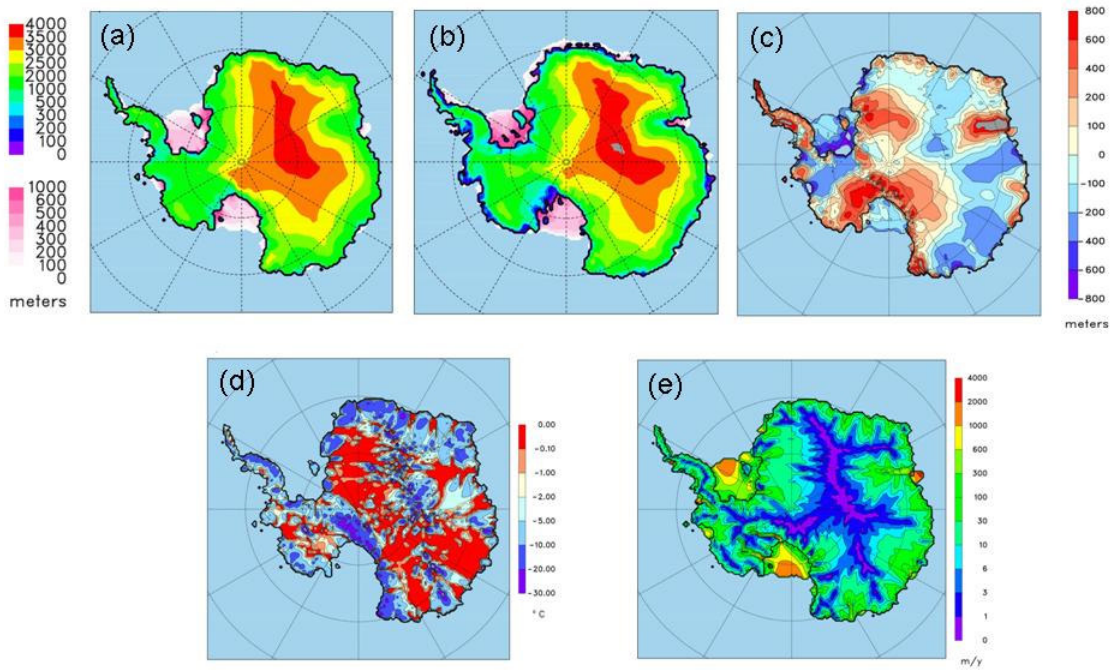

Figure S2. (**a**) Model ice elevations (grounded) and thicknesses (floating), for modern (0 ka) in the nominal run shown in Fig. 2b. (**b**) As (a) for modern observed Antarctica[1]. (**c**) Differences a-b, model minus observed. (**d**) Model basal temperatures relative to the pressure melt point (ºC, red ≈ melting) at 0 ka. (**e**) Model ice surface speeds (m y^{-1}) at 0 ka.

General error magnitudes in modern ice elevations (Fig. S2c) are on the same order as those found in other Pleistocene models[6,7]. There are large errors over the Lambert Graben/Prydz Bay (~80ºS, 70ºE) where the model grounding line is too far advanced down the bay, and conversely for the innermost Ronne Ice Shelf. Elsewhere, the agreement with modern grounding-line locations is good, especially in the Ross Embayment. The two largest islands (Roosevelt and Berkner) under the major shelves are captured. Ice elevations are too high over much of western WAIS (grounded Siple Coast and Rockefeller Plateau), perhaps due to too much bed friction with not enough bed area reaching the melt point, resulting from the model's lack of basal hydrology and liquid water flowing originating upstream[44]. Floating ice thicknesses in the Ross and Filchner-Ronne shelves are somewhat thinner than observed. Both of these errors are partially corrected in sensitivity experiments described below in SI sections 6-7. Future work will aim at further improving these aspects, focusing on basal hydrology, sediment distribution, and the long-term evolution leading up to the modern snapshot at 0 ka.

Model ice speeds (Fig. S2e) generally compare well with modern balance velocity maps and measurements[45,46]. In both panels (d) and (e), hints of poorly resolved ice "streams" are seen in the Siple Coast and Prydz Bay regions; these are resolved much better in the higher-resolution nested run shown in Fig. 3f and Supplementary Videos V3-4. Simulated ice velocities of the modern Byrd Glacier (80.3ºS, 160ºE) and some of the Siple streams in Fig. 3f are somewhat faster than observed[47-49], perhaps because of neglect of longitudinal stresses or incorrect basal stiffness.

3. Simulated Conditions at Specific Points in the Ross Embayment

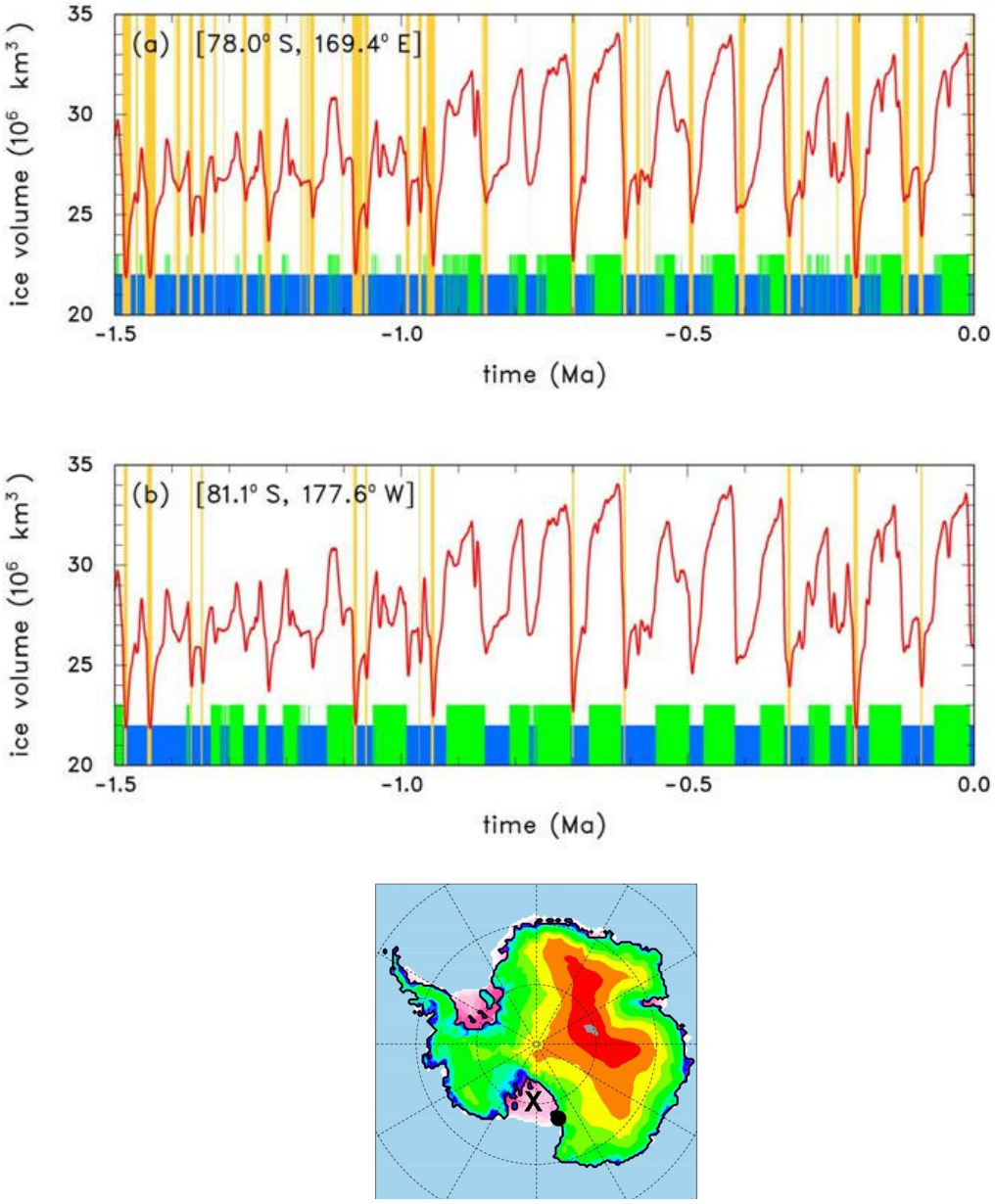

Figure S3. Total Antarctic ice volume for the last 1.5 Myr of our nominal long-term simulation. (**a**) Lower colored boxes indicate conditions at a single location one grid box to the east of the ANDRILL AND-1B core[11] (black dot in map) in McMurdo Sound. Yellow = open ocean, blue = floating shelf, green = grounded ice. The eastward shift was made to avoid poorly resolved Ross Island shorelines. (**b**) Same as (a) except for grid location (81.1ºS, 177.6ºE, black X in map) in the central region of the Ross Embayment.

The upper panel (a) in Fig. S3 is the same as in Fig. 2c, except the yellow boxes (open ocean) are extended upwards to show correlations with ice-volume minima. In the lower panel, open-ocean events at the more central Ross-Sea location are more infrequent, and with few exceptions occur only for near-complete WAIS collapses (total ice volume < ~23×10^6 km^3). A core drilled at this site would have the potential of uniquely identifying WAIS collapses, assuming other requirements such as sediment preservation are met.

4. Marine Isotope Stage 31

Sediment cores near Ross Island[11, 21] and elsewhere around Antarctica[50] indicate strong circum-Antarctic warming during Marine Isotope Stage 31 ~1.08 to 1.06 Ma. Drastic ice-shelf retreat and seasonally open water around Ross Island at this time[11,21] coincide with one of the strongest austral summer insolation anomalies of the Pleistocene[20]. The model time series around MIS-31 (Fig. 2c) has a distinct precessional (~20 kyr) component due to the influence of austral summer insolation, and agrees well with the phase of the 20 kyr cyclicity in off-shore records[21]. The snapshot at 1.079 Ma (Fig. 3b) shows peak collapse of nearly all marine ice in West Antarctica. Although the actual degree of collapse is not known, the retreat of shelf ice far southward of Ross Island agrees with data[10, 11]. In Global Climate Model (GCM) simulations of MIS-31 climate, with the Ross Ice Shelf removed and with ocean melting under sea ice increased to match our sub-ice-shelf parameterization[51], we find ~4ºC summer warming and open ocean near Ross Island in full agreement with interpretations based on diatom assemblages[21]; however, this warming is insensitive to the size of WAIS specified in the GCM, so the results do not shed light on the degree of collapse.

5. Sensitivity Experiments: Southern Hemispheric Solar Insolation Forcing

Our use of deep-sea-core benthic $\delta^{18}O$ as the main long-term forcing is empirical and pragmatic. The $\delta^{18}O$ time series has two properties that are consistent with the new AND-1B record of Antarctic response[11]: its higher-frequency fluctuations mainly have ~40 kyr periodicity, and it has a long-term cooling trend over the last 5 Myr from the early-to-mid Pliocene (~5 to 3 Ma) to the late Pleistocene glacial cycles (~1 to 0 Ma). The fact that our model response mirrors these basic features is not surprising; instead, the main substantive outcome of this study is that (i) the simulations are in reasonable agreement not only with AND-1B, but also with observed last glacial (15 ka) to modern extents, and implied drastic WAIS retreats in a few previous interglacials, and (ii) this can be achieved with plausible values of past and present sub-ice oceanic melt rates.

However, our use of $\delta^{18}O$ to drive long-term forcing variations, with an additional slight influence of austral summer insolation, is really a hypothesis. It is clearly testable by further work with global climate and regional ocean dynamical models. Here, as a very crude test of alternate forcings, we performed two sensitivity tests using only Southern Hemispheric insolation as long-term forcing, with no $\delta^{18}O$ influence (Fig. S5). Using annual insolation anomalies (solid blue curve), the last WAIS deglacial retreat is now quite unrealistic, beginning and ending too early (~20 to 10 ka) compared to observed (~10 to 3 ka[24,25]). Using summer insolation anomalies (dashed blue curve), similar problems arise for the last deglacial retreat. This bears out our reasoning in the Methods section, that the observed timing of the last glacial maximum and retreat of WAIS must have been forced primarily by far-field influences correlated with benthic $\delta^{18}O$.

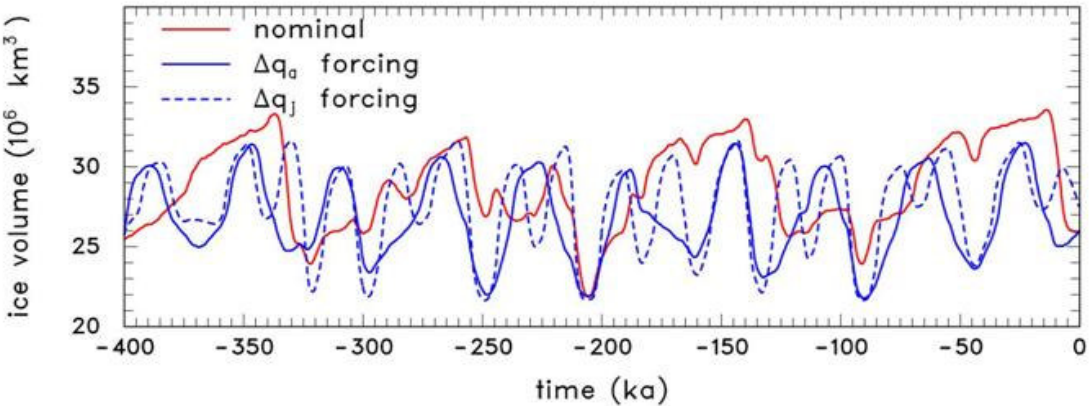

Figure S5. Simulated Antarctic ice volume for the last 400 kyr. **Red:** nominal long-term simulation. **Solid blue:** with austral *annual mean* insolation anomaly at 80ºS (Δq_a, W m^{-2}) instead of deep-sea-core ($\delta^{18}O$) as the main long-term forcing of sub-ice melt, i.e., with the $\Delta s/85$ term in Eq. (6) of the Methods section replaced by (0.1 Δq_a - 0.3) / 0.9. **Dashed blue:** with austral *summer* (January) insolation anomaly at 80ºS (Δq_j, W m^{-2}), i.e., with $\Delta s/85$ in Eq. (6) replaced by (0.1 Δq_j - 1) / 5. These expressions are adjusted to maintain roughly the same mean ice-sheet sizes and peak-to-peak amplitudes as in the nominal run.

6. Sensitivity Experiment: Last Deglacial History

The deglacial history of Antarctica over the last ~15,000 years is relatively well known, and provides valuable data for model validation. In particular, the sequence of grounding line retreat across the Ross Embayment has been deduced from local geologic evidence as similar to a "swinging gate", with fairly smooth retreat from near-continental-shelf edges ~15 ka to close to present after ~3 ka[24,25]. In our nominal long-term run, the model's Ross-Embayment retreat resembles a swinging gate (shown in Supplementary Video V1), but is too sudden and occurs mostly between 10 ka and 8 ka.

The retreat is noticeably improved in a sensitivity experiment with increased buttressing of ice shelves. This experiment was motivated by several small ice rises observed just downstream of the modern Siple Coast grounding line (Horgan and Anandakrishnan[52] and H. Horgan, pers. comm.), which are not resolved by the 40 km grid. We added a parameterization of sub-grid pinning by small bedrock rises, in which additional basal stress is applied at the bottom of floating ice for water column thicknesses $h_w \leq 300$ m; i.e., the basal sliding coefficient is ramped linearly from 15% of the grounded-ice value (for $h_w = 0$) to no resistance (for $h_w \geq 300$). This by itself would cause buttressing to increase and grounding lines to advance unrealistically, so to compensate, we increased the grounding-line fluxes given by Eq. (S1) by a factor of 10. This leaves grounding-line locations mostly unchanged, and causes a general thickening of shelf ice, improving the underestimation of modern thicknesses in the nominal run (actually overcorrecting for the Ronne). Loosely speaking, these modifications increase the amount of "compression" in the major ice shelves between the grounding-line input flux and the downstream resistance.

The modeled sequence through the last deglaciation (after a 400 kyr run) is shown in Fig. S6. The sequence of grounding-line retreat in the Ross Embayment is now much smoother and lasts from ~10 ka to 2 ka, in much better agreement with observations[24,25].

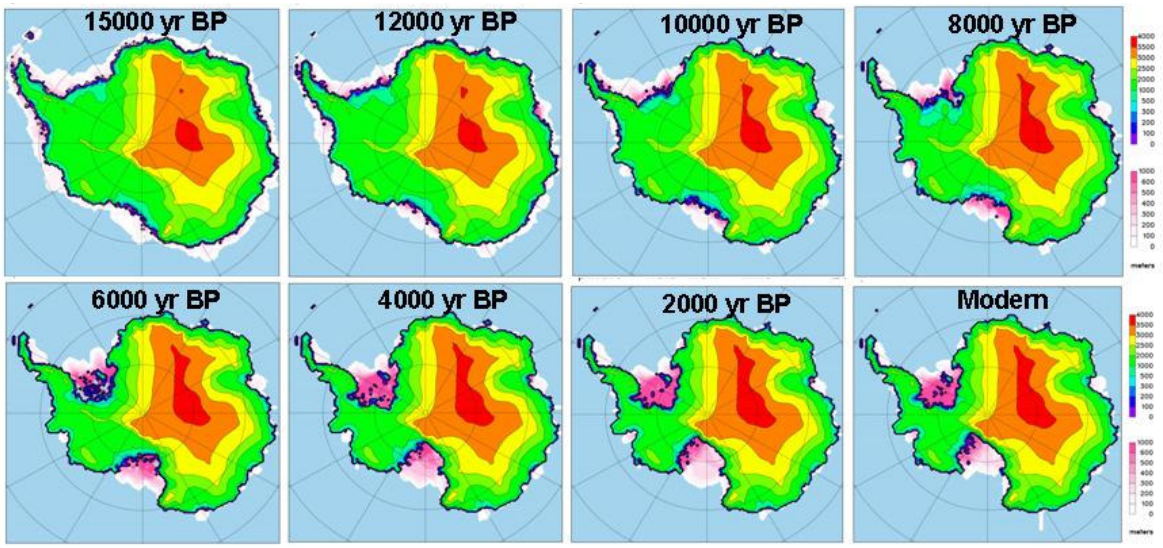

Figure S6. Snapshots of ice elevations (grounded) and thicknesses (floating) through the last deglaciation in the sensitivity run described above with sub-grid ice-shelf pinning and increased grounding-line flux coefficient (see text). These changes considerably improve the realism of grounding-line retreat in the Ross Embayment.

7. Sensitivity Experiment: West Antarctic Ice Sheet Profiles

The largest departure from modern observed conditions in our nominal simulation is the overestimation of ice thicknesses over WAIS (SI section 2). This problem is common to earlier models[6, 7] and has been ascribed to underestimated basal sliding, perhaps due to insufficient lubrication or too much bed area below freezing[44]; also there may be insufficient overall transport by ice streams, which are barely resolved with a 40 km grid. The overestimation of ice thickness is exacerbated at the last glacial maximum (15 ka for Antarctica), when expanded ice cover over the Ross Embayment remained thin far inland from the grounding line, only a few hundred meters thicker than modern in many areas[53,54].

This study does not resolve the problem, which we regard as a major future challenge in this field. Its resolution will likely require better knowledge of sediment vs. bedrock and frozen vs. thawed bed distributions under WAIS, and better understanding of the large-scale role of ice streams (cf. SI section 8). Our main concern here is that long-term WAIS evolution and our 5 Myr results do not depend acutely on details of WAIS sediment distributions or ice profiles. To test this, we performed several sensitivity experiments with increased basal sliding coefficients under WAIS that produce more realistic (lower) ice profiles. One such experiment is described below, with little change in the long-term ice sheet variations (Fig. S7A). This suggests that the main results of this paper are robust, and will not be changed substantially by further tuning of bed conditions to reduce modern biases.

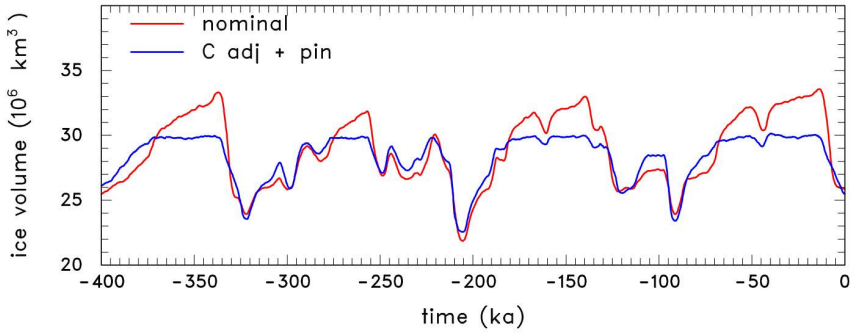

Figure S7A. Red: Total ice volume in last 400 kyrs of the nominal model simulation. **Blue:** Sensitivity experiment with adjustments to WAIS basal sliding coefficients, and also sub-grid ice-shelf pinning (see text).

The main change in Fig. S7A (blue curve) is an increase in the basal sliding coefficient B over WAIS sediment areas to 10^{-5} (from 10^{-6}) m a^{-1} Pa^{-2}, except in the Filchner-Ronne drainage area where it is kept at 10^{-6}. In addition, over Siple Coast drainages, some sliding is permitted for frozen beds, with B reduced only to 10^{-7} m a^{-1} Pa^{-2} (not to ~zero; cf. Parizek et al.[44]). This run also includes the sub-grid pinning parameterization described in SI section 6. The time series of total ice volume is much the same as the nominal run, except that maximum glacial volumes are capped at ~30 x 10^6 km^3. The

larger nominal values are due to ~km thicker ice over much of WAIS during glacial periods.

Over much of the Siple Coast region, grounded ice elevations in the new simulation are ~500 m lower (Figs. S7B amd S7C). Upstream from the modern grounding line, elevations in the new run are a few hundred to several hundred meters higher at 15 ka than modern, still somewhat more than observed at some locations[53,54], but more realistic than the larger 15 ka vs. modern differences in the nominal run.

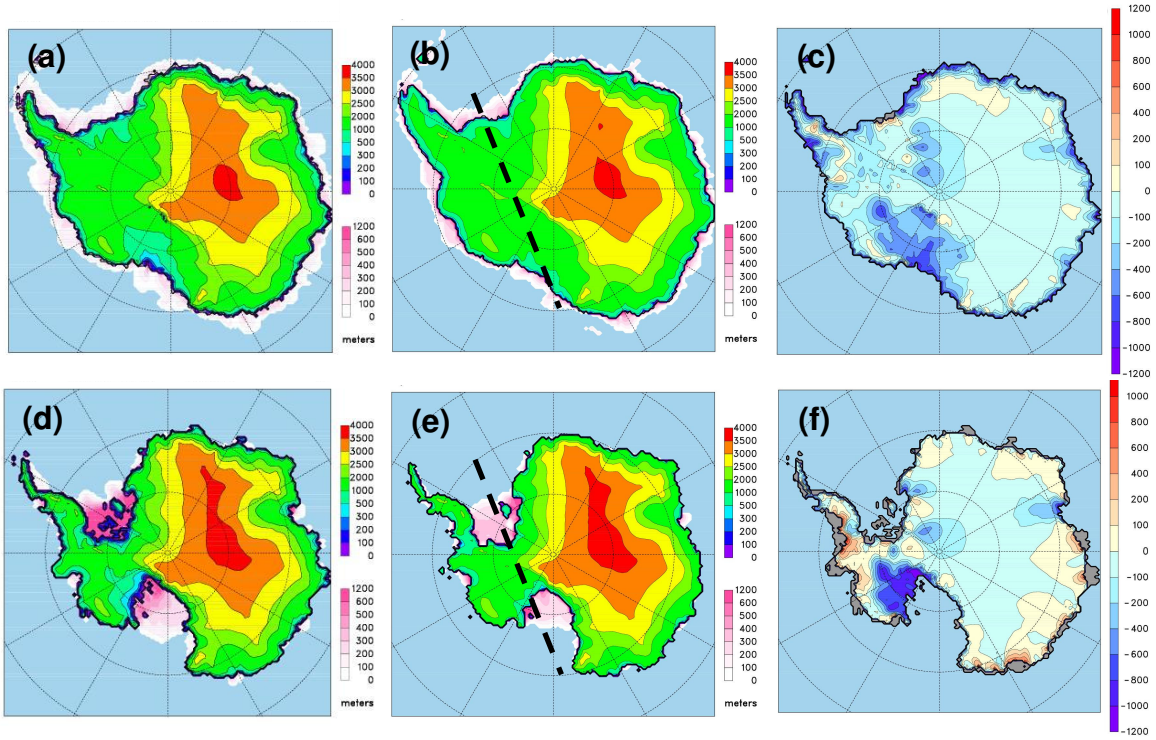

Figure S7B. **(a)** Ice elevations (grounded) and thicknesses (floating) at 15 ka, in a sensitivity test with adjustments to the basal sliding coefficient under WAIS areas, and also sub-grid ice-shelf pinning (see text). **(b)** At 15 ka, in the nominal model. **(c)** Difference (a minus b). **(d) to (f)** Same as (a) to (c) except for modern. The cross section for Fig. S7C is shown in (b) and (e) as a thick dashed line.

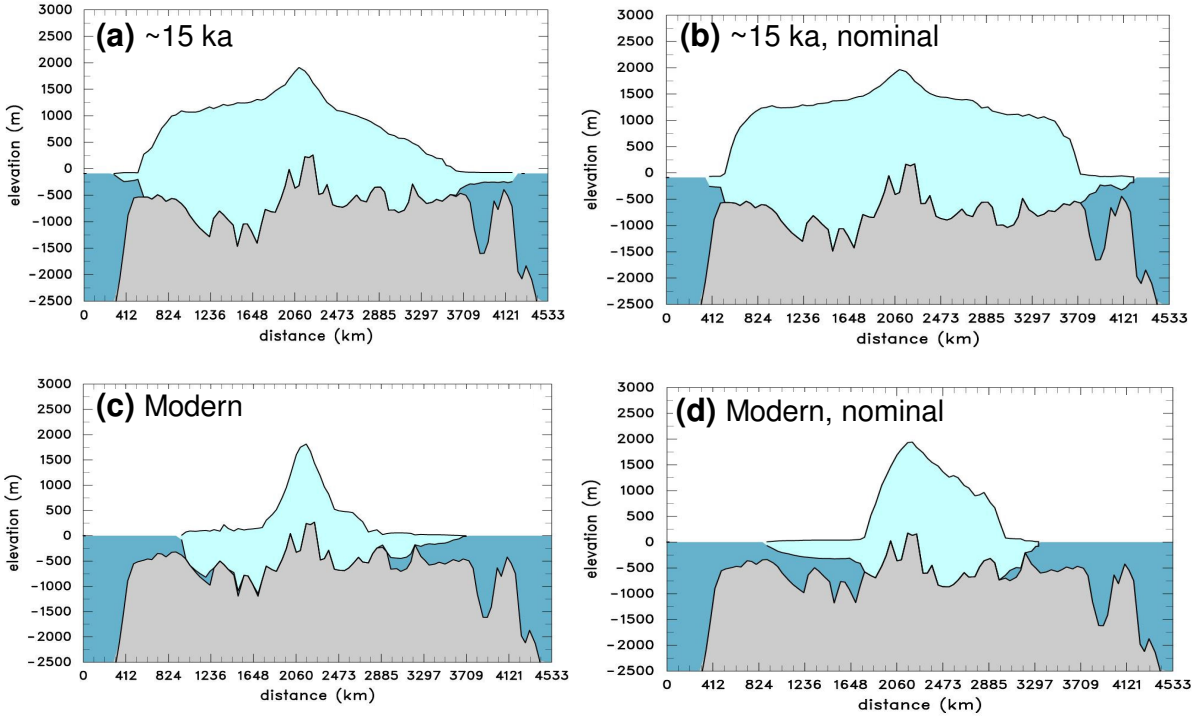

Figure S7C. Cross sections of ice and bedrock through WAIS, from the Weddell Sea (left) to the Ross Sea (right), [70ºS,40ºW] to [70ºS,178ºE] as shown in Fig. S7B(a,b,d,e). **(a)** At ~15 ka, in a sensitivity experiment with adjustments to the basal sliding coefficient under WAIS areas, and also sub-grid ice-shelf pinning (see text). **(b)** At ~15 ka, in the nominal model. **(c) and (d)** Same as (a) and (b) except for modern.

8. Sensitivity Experiment: Combined Flow Equations in Grounded Areas

As described in SI section 1, for efficiency in most runs we do not use the heuristically combined sheet (SIA) and shelf-flow equations everywhere[12], but apply them separately to grounded and floating regions respectively. This simplification is likely to have most impact in the transition zone upstream of grounding lines, where longitudinal stresses in ice streams may be important for the large-scale evolution. Without longitudinal stresses, the modern Siple Coast network of ice streams is simulated quite well in our 10-km nested runs (Fig. 3, and videos V3–V4) and even somewhat in our 40 km runs, and stems from the positive feedback between basal sliding, frictional heating and thawing at the bed[55]. However, the role of ice streams and the level of ice-stream detail needed for modeling long-term ice-sheet evolution are not well known, and are important ongoing research areas. Here, we take a step in this direction, by performing a sensitivity run with the heuristic sheet-shelf-flow iterative combination applied in grounded as well as floating regions. It would be too computationally expensive to do this over the entire domain (and wasteful, because in our coarse-grid model, non-SIA stretching flow is negligible over most of EAIS with low basal sliding coefficients $B = 10^{-10}$ m a^{-1} Pa^{-2}). Instead, we apply the combination only where $B > 0.5\ 10^{-8}$ m a^{-1} Pa^{-2}, which includes all thawed sediment beds (much of WAIS). This modification is in addition to those for the sensitivity tests described in SI sections 6 and 7. Results for the last 400 kyr are shown in the figures below.

The time series of ice volume (Fig. S8A), mainly reflecting variations in WAIS extent, is essentially unchanged by the inland combined calculations, both for interglacial and glacial states. With this modification, grounding lines in the Weddell and Ross embayments tend to be more advanced, as seen for modern in Fig. S8B. However, the amount of grounding-line shift is relatively small, and is typical of those induced by many small parameter changes in the model that produce only minor changes in the long-term evolution.

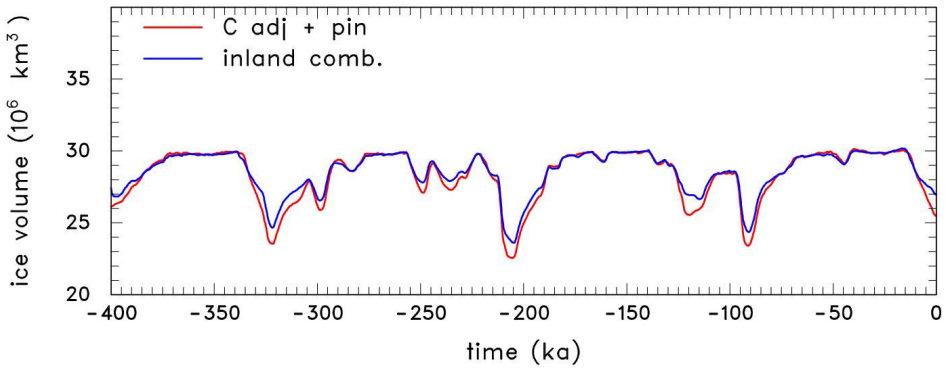

Figure S8A. Red: Total ice volume in the previous sensitivity experiment described in SI section 7 with adjusted WAIS basal sliding coefficients and sub-grid ice-shelf pinning. **Blue:** With those changes, and also with combined sheet-shelf-flow calculations in regions with basal sliding coefficient $B > 0.5\ 10^{-8}$ m a^{-1} Pa^{-2} (which includes most of inland WAIS).

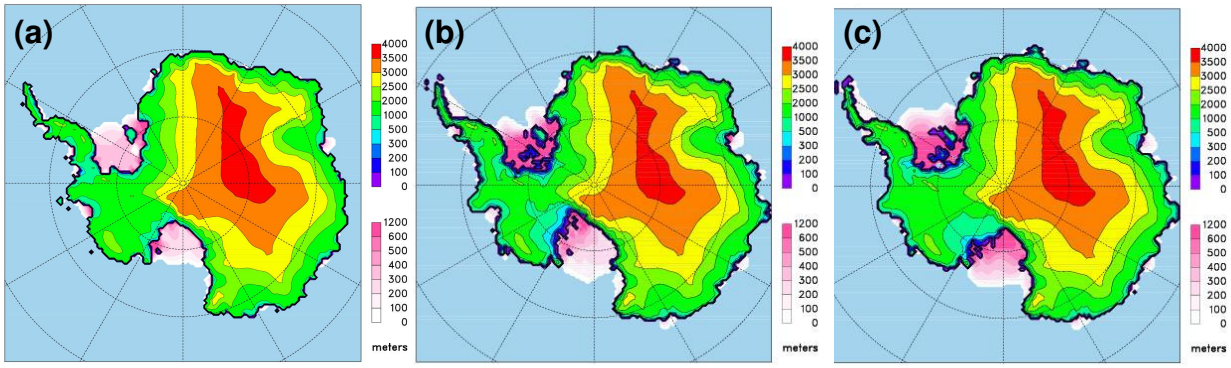

Figure S8B. Snapshots of modern ice elevations (grounded) and thicknesses (floating). **(a)** In the nominal model simulation. **(b)** In the previous sensitivity experiment described in SI section 7 with adjusted WAIS basal sliding coefficients and sub-grid ice-shelf pinning. **(c)** With those changes, and also with combined sheet-shelf flow calculations in regions with basal sliding coefficient $B > 0.5\ 10^{-8}$ m a^{-1} Pa^{-2} (which includes most of inland WAIS).

SUPPLEMENTARY REFERENCES

38. Rommelaere, V. & Ritz, C. A thermomechanical model of ice-shelf flow. *Ann. Glaciol.* **23**, 13-20 (1996).
39. Schoof, C., Hindmarsh R. & Pattyn, F. Benchmarks and intercomparison program for marine ice sheet models. Abstract EGU2007-A-04644, *European Geosciences Union,* General Assembly, Vienna, http://homepages.ulb.ac.be/~fpattyn/mismip and http://meetings.copernicus.org/egu2007/annotation.html (2007).
40. Pollard, D. & DeConto, R. Grounding line behavior in a heuristally coupled ice-sheet shelf model. Abstract EGU2007-A-03103, *European Geosciences Union*, General Assembly, Vienna, http://meetings.copernicus.org/egu2008/annotation.html (2008).
41. Pattyn, F., Huyghe, A., De Brabander S. & De Smedt, B. The role of transition zones in marine ice sheet dynamics. *J. Geophys. Res.-Earth Surface*, **111**, F02004, doi:10.1029/2005JF000394 (2006).
42. Farrow, D.E. & Stevens, D.P. A new tracer advection scheme for Bryan and Cox type ocean general circulation models. *J. Phys. Oceanogr.* **25**, 1731-1741 (1995).
43. Pollard, D., DeConto R. M. & Nyblade, A. A. Sensitivity of Cenozoic Antarctic ice sheet variations to geothermal heat flux. *Glob. Planet. Change* **49**, 63-74 (2005).
44. Parizek, B.R., Alley, R. B. & Hulbe, C. L. Subglacial thermal; balance permits ongoing grounding-line retreat along the Siple Coast of West Antarctica. *Ann. Glaciol.* **36**, 251-256 (2003).
45. Bentley, C.R., Rapid sea-level rise from a West Antarctic ice-sheet collapse: a short-term perspective. *J. Glaciol.* **44**, 157-163 (1998).
46. Huybrechts, P., Steinhage, D., Wilhelms F. & Bamber, J. Balance velocities and measured properties of the Antarctic ice sheet from a new compilation of gridded data for modelling. *Ann. Glaciol.,* **30***,* 52-60 (2000).
47. Whillans, I. M., Chen, Y. H., Vanderveen C. J. & Hughes, T. J. Force Budget .3. Application to 3-Dimensional Flow of Byrd Glacier, Antarctica. *J. Glaciol.* **35**, 68-80 (1989).

48. Joughin, I. & Tulaczyk, S. Positive mass balance of the Ross Ice Streams, West Antarctica. *Science* **295**, 476-480 (2002).

49. Rignot, E. *et al*. Recent Antarctic ice mass loss from radar interferometry and regional climate modelling. *Nature Geoscience* **1**, 106-110 (2008).

50. Villa G., C. *et al*. A Pleistocene warming event at 1 Ma in Prydz Bay, East Antarctica; Evidence from ODP site 1165. *Palaeogeogr., Palaeoclim., Palaeoecol,* **260**, 230-244 (2008).

51. DeConto, R. *et al.*. Antarctic climate-cryosphere response to extreme orbital forcing during Marine Isotope Stage 31. *EOS Transactions*, American Geophysical Union **88**, Fall Meeting Suppl., Abstract PP41F-07, http://www.agu.org/meetings/fm07/waisfm07.html (2007).

52. Horgan, H. J. & Anandakrishnan, S. Static grounding lines and dynamic ice streams: Evidence from the Siple Coast, West Antarctica. *Geophys. Res. Lett.*, **33**, L18502, doi:10.1029/2006GL027091 (2006).

53. Waddington, E. D. *et al.* Decoding the dipstick: Thickness of Siple Dome, West Antarctica, at the Last Glacial Maximum, *Geology* **33**, 281-284 (2005).

54. Ackert, R. P., Mukhopadhyay, S., Parizek B. R. & Borns, H. W. Ice elevation near the West Antarctic Ice Sheet divide during the last glaciation. *Geophys. Res. Lett.* **34**, L21506, doi:10.1029/2007GL031412 (2007).

55. Payne, A. J. A thermomechanical model of ice flow in West Antarctica. *Clim. Dyn.* **15**, 115-125 (1999).

56. Siegert, M. J. *et al.* Ice flow direction change in interior West Antarctica. *Science* **305**, 1948-1951 (2004).

SUPPLEMENTARY VIDEO LEGENDS

Video V1. This animation shows model surface elevations of grounded ice and thicknesses of floating ice (m), every 1000 years through the last 400 kyr of the long-term simulation shown in Fig. 2b. The major ~100 kyr glacial-interglacial cycles are prominent. As discussed in the text, there is a tendency for WAIS to vary "one-dimensionally", i.e., with its different sectors usually retreating and expanding in unison, resulting in just one configuration for a given total ice volume. Both this video and V2 show that collapsed WAIS states are relatively short lived, and that transitions into and out of them are usually rapid, taking one to a few thousand years.

Video V2. Same as V1 except every 2000 years for the period 1.7 Ma to 0.6 Ma, which includes the Marine Isotope Stage 31 event ~1.08 to 1.06 Ma.

Video V3. This animation shows surface ice velocities (m y^{-1}) every 50 years in the higher-resolution (10 km) nested simulation for modern conditions (Fig. 3f,i). For nested runs, the model physics are identical to the continental model. Boundary conditions of ice thickness and velocity at the edges of the domain, and initial conditions in the interior are obtained by interpolating the course-grid (40-km) results for 0 ka. Over the 8800 years of this nested run, ice and grounding-line configurations continue to evolve away from the initial 0 ka "snapshot" state, which is not consistent with the fixed 0-ka boundary conditions applied at the edges. Also, the finer resolution does change the model behavior somewhat, such as (unrealistically) greater extents of ice-shelf edges. Nevertheless, as also seen in Fig. 3f, Siple Coast ice streams are surprisingly well resolved, and the network sometimes bears some correspondence to the actual streams. Although the placement of the streams is loosely controlled by shallow ridges and valleys in the prescribed bed topography[1], the narrowness of the streams, network morphology, and the position of the grounding line itself are primarily a consequence of the model physics. Over the course of this animation, the Siple Coast network is highly dynamic, with ice streams first becoming established and then stagnating and restarting on ~10^3-year time scales. Similar behavior was found in a WAIS ice flow model by Payne[55], and is reminiscent of the recent stagnation of the Kamb Ice Stream (formerly C) and other century-to-millennial scale switching[31,56].

Video V4. Same as V3 except showing temperatures at the ice-bed interface relative to the pressure melt point (ºC). Red shows the base essentially at the melt point, where basal sliding can occur. Below -0.5ºC, basal sliding is zero. The beds of active Siple Coast ice streams and their source regions are at the melt point, and are frozen over much of the intervening areas[55]. The same is true for major outlet glaciers flowing through the Transantarctic Mountains.